Popular benchmarks of nonlinear shell analysis solved by 1D and 2D CUF-based finite elements

Paper submitted for the Special Issue celebrating the 75th Anniversary of Professor J.N. Reddy

Popular benchmarks of nonlinear shell analysis solved by 1D and 2D CUF-based finite elements

E. Carrera*, A. Pagani†, R. Augello‡, B. Wu§

Mul^2 Group
Department of Mechanical and Aerospace Engineering, Politecnico di Torino
Corso Duca degli Abruzzi 24, 10129 Torino, Italy.

Abstract: *This research work deals with the analysis of shell structures in the large displacement and rotation field adopting one-dimensional (1D) and two-dimensional (2D) unified models. Namely, higher-order beam and shell theories accounting for geometrical nonlinearities are formulated by employing a unified framework based on the Carrera Unified Formulation (CUF) and a total Lagrangian approach. Thus, a Finite Element (FE) approximation is used along with a Newton-Raphson method and an arc-length path-following approach to perform nonlinear analyses. Low- to higher-order beam and shell theories are used to evaluate the nonlinear equilibrium path, and results are compared between the two models, with reference solutions coming from literature or 2D and three-dimensional (3D) models from NASTRAN. Convergence analyses show how CUF 1D models are able to describe the geometrical nonlinear behavior of analyzed structure with a lower number of Degrees of Freedom (DoFs) than 2D and 3D models.*

Keywords: Carrera unified formulation; Geometrical nonlinearities; Beam and shell theories; Convergence analyses.

---

1 Introduction

Shell structures are widely adopted in various engineering fields and, as a matter of fact, modern design processes demand for accurate prediction of their mechanical behaviour. When external loading conditions become large, shell structures are prone to suffer large rotations, and the adoption of models able to describe internal stress states as well as complex displacement fields in this condition is of paramount importance. For this purpose, designers often rely on three-dimensional (3D) Finite Element (FE) simulation to obtain a reasonable

*Professor of Aerospace Structures and Aeroelasticity
†Assistant Professor. Corresponding author. E-mail: alfonso.pagani@polito.it
‡Post Graduate Research Assistant. E-mail: riccardo.augello@polito.it
§Postdoctoral Fellow. E-mail: bin_wu@polito.it

structural response. The need to reduce the computational cost of the analysis of structures with complex geometry, such as thin-walled and shell-like components, pushed scientists and researchers to develop refined one-dimensional (1D) and two-dimensional (2D) theories for the modeling of such structures, with an acceptable loss of accuracy. The main goal of this research work is a comparison between 1D and 2D shell models developed in a unified manner, for the geometrical nonlinear analysis of shell structure.

Beam models represent a suitable solution for the analysis of structure in which length is dominant compared to the other dimensions. The interest in the development of beam models is high due to the possibility of its adoption in many engineering fields, such as aerospace engineering for the analysis of aircraft wings of helicopter blades, civil engineering for slender bridges, or automotive engineering for transmission shafts. Interestingly, the lower computational cost compared to 2D and 3D models, makes beam models the optimal solution for the analysis of slender structures. The best-known beam theories, considered as classical beam models, are those by Euler [1] and Timoshenko [2, 3]. These models are reliable when dealing with slender and compact structure. In fact, the former does not account for shear deformations, whereas the latter considers a uniform shear distribution along the cross-section of the beam-like structure. On the contrary, when dealing with structures in which the cross-section deformability plays an important role in the overall static behavior, the adoption of more sophisticated 1D models is needed, see [4]. For this reason, higher-order 1D models were developed to overcome these limits. A comprehensive discussion about higher-order beam models for the linear analysis of metallic structures can be found in the paper by Carrera *et al.* [5]. A comprehensive review of beam (including plate) theories was presented by Kapania and Raciti [6, 7]. An overview of existing beam FEs was made by Reddy [8], where beam elements based on classical and higher-order theories were described, and the problems of shear locking and locking-free beam elements were discussed. As further examples, Petrolito [9] and Eisenberger [10] dealt with the exact stiffness matrix analysis of a high-order beam element: the refined displacement field was based on a cubic variation of the axial displacement over the cross-section of the beam, and the importance of higher-order terms in case of short beams was underlined. The Generalized Beam Theory (GBT) was used to implement beam theories accounting for the in-plane cross-section deformations, and shell-type results were obtained by using appropriate cross-section shape functions describing the beam displacement field. GBT was also used by Rendek and Baláž [11], for the static analysis of thin-walled beams and comparisons with experimental results. The adoption of higher-order beam models is required when the structures is in the large deflection and rotation field. For instance, Frischkorn and Reese [12] used a eight-node beam element with only displacement Degrees of Freedoms (DoFs) for the nonlinear modeling in the large displacement field. Vieira *et al.* [13] proposed an higher-order beam model for the geometrical nonlinear analysis of thin-walled structure, with an opportune integration over the cross-section.

As far as the 2D model is concerned, a variety of shell theories were proposed in the last decades. The classical theories come from the pioneering works by Cauchy [14], Poisson [15], Kirchhoff [16], Love [17] and by Reissner [18] and Mindlin [19]. To overcome the approximations and assumptions made by classical theories, for example when dealing with composite structures or, in general, when the through-the-thickness strains and stresses highly afflict the overall static behavior, a series of higher-order 2D theories have been developed. For example, Reddy [20] reviewed and described the mechanics of laminated 2D structures (indluding plate theory). Reddy and Liu [21] developed a shear model accounting for a parabolic distribution of the trhough-the-thickness transverse shear strains. A parabolic shear strain distribution was assumed also by Kulkarni and Bakora [22] to develope an eigth node FE of

a shell element with piezo-elettric effects. Moreover, Liew and Lim [23] resorted to a cubic distribution of the shear strains to evaluate the vibration caharacteristics of thick cylindrical shallow shells. The literature about the adoption of higher-order shell models for the geometrical nonlinear analysis is wide. Hughes and Liu [24] developed a nonlinear FE formulation for the quasistatic analysis of shells in the large strains and rotations field. Surana [25] used a total lagrangian approach for the 3D curved shell elements. Large membrane strains were anayzed by the developed model from Hughes and Carnoy [26]. A shell model with six DoFs per node was been developed by Park *et al.* [27] for the accurate description of the strain field in the geometrical nonlinear analysis. The large deformation field of both single-layered and laminated shells was been investigated by Lee and Kanok-Nukulchai [28], using the arc-length method to follow any load-displacement paths. Finally, Providas and Kattis [29] adopted the well-known von Kármán approximations for the geometrical nonlinear analysis of thin shells. The 1D and 2D shell models and the related nonlinear analysis proposed in this work are based on the Carrera Unified Formulation (CUF) [30, 31]. According to CUF, any theory of structures can degenerate into a generalized kinematics that makes use of an arbitrary expansion of the generalized viariables. In this manner, the nonlinear governing equations and the related FE arrays of the beam and shell theories are written in terms of *fundamental nuclei*. These fundamental nuclei represent the basic building blocks that, when opportunely expanded, allow for the straightforward generation of low- and high-order finite beam and shell elements. CUF has been utilized for many engineering problems over the last few years; e.g., composite structures [32], rotating blades and rotors [33], civil engineering structures [34], aerospace constructions [35, 36], and multi-field problems [37], among the others. CUF was extended to geometrical nonlinear problems, for both metallic and composite structure regarding the static [38, 39] and vibration analysis [40, 41]. Here, the formulation is further extended to deal with the geometrical analysis of shell structures, which formulation was presented by [42].

This paper is organized as follows: (i) first, preliminary and introductory information about 1D and 2D models are reported in Section 2, including the geometrical and constitutive expressions for elastic metallic materials, the Green-Lagrange nonlinear geometrical relations, CUF, and the related FE; (ii) subsequently, Section 3 briefly reports the solution adopted in this work for the resolution of the geometrical nonlinear FE equations; (iii) then, numerical results are discussed for a pinched cylinder and a cylindrical panel, including a comparison with literature results and results from the commercial software NASTRAN in Section 4; (iv) finally, the main conclusions are drawn.

2 Carrera unified formulation

One-dimensional (1D) beam and two-dimensional (2D) shell models for a generic cylindrical structure are described hereafter. Figure 1 shows the 1D model, with the cross-section Ω, which lays on the xz-plane of a Cartesian reference system (x, y, z). As a consequence, the beam axis is placed along y. The transposed displacement vector is introduced in the following:

$$\mathbf{u}(x,y,z) = \left\{ \begin{array}{ccc} u_x & u_y & u_z \end{array} \right\}^T \tag{1}$$

The stress, $\boldsymbol{\sigma}$, and strain, $\boldsymbol{\epsilon}$, components are expressed in vectorial form with no loss of generality,

$$\boldsymbol{\sigma} = \left\{ \begin{array}{cccccc} \sigma_{xx} & \sigma_{yy} & \sigma_{zz} & \sigma_{xz} & \sigma_{yz} & \sigma_{xy} \end{array} \right\}^T, \quad \boldsymbol{\epsilon} = \left\{ \begin{array}{cccccc} \epsilon_{xx} & \epsilon_{yy} & \epsilon_{zz} & \epsilon_{xz} & \epsilon_{yz} & \epsilon_{xy} \end{array} \right\}^T \tag{2}$$

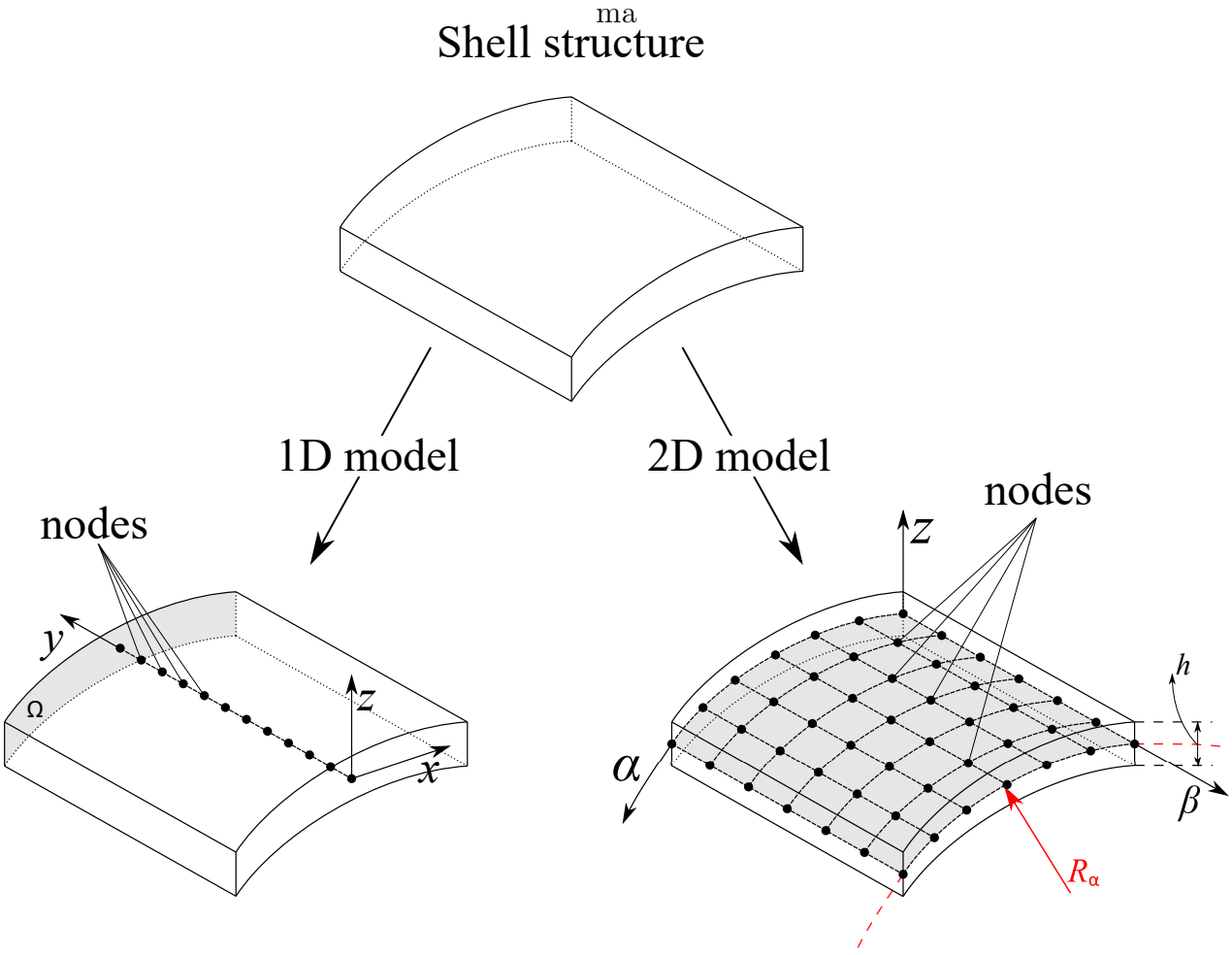

Figure 1: The modeling of a generic shell structure using both 1D and 2D models. For 1D model, y is the direction of the beam axis, whereas for the 2D model z is the shell thickness coordinate.

The 2D model of a generic shell structure is also reported in Fig. 1, along with its curvature radius R_α and thickness h. The geometry is described using a orthogonal curvilinear reference system (α, β, z), in which α and β are the two in-plane directions and z represents the through-the-thickness coordinate. The three-dimensional (3D) displacement transposed vector $\mathbf{u}$ of a given point in the continuum shell is:

$$\mathbf{u}(\alpha,\beta,z) = \left\{ \begin{array}{ccc} u_\alpha & u_\beta & u_z \end{array} \right\}^{\mathrm{T}}, \tag{3}$$

The transposed strain ($\boldsymbol{\epsilon}$) and stress ($\boldsymbol{\sigma}$) vectors defined in the curvilinear reference system are:

$$\boldsymbol{\sigma} = \left\{ \begin{array}{cccccc} \sigma_{\alpha\alpha} & \sigma_{\beta\beta} & \sigma_{zz} & \sigma_{\alpha z} & \sigma_{\beta z} & \sigma_{\alpha\beta} \end{array} \right\}^{\mathrm{T}}, \quad \boldsymbol{\epsilon} = \left\{ \begin{array}{cccccc} \epsilon_{\alpha\alpha} & \epsilon_{\beta\beta} & \epsilon_{zz} & \epsilon_{\alpha z} & \epsilon_{\beta z} & \epsilon_{\alpha\beta} \end{array} \right\}^{\mathrm{T}}, \tag{4}$$

2.1 Geometrical and constitutive relations

As far as the geometrical relations are concerned, the Green-Lagrange nonlinear strain components are considered. Therefore, the displacement-strain relations are expressed as

$$\boldsymbol{\epsilon} \;=\; \boldsymbol{\epsilon}_l + \boldsymbol{\epsilon}_{nl} \;=\; (\mathbf{b}_l + \mathbf{b}_{nl})\mathbf{u} \tag{5}$$

where $\mathbf{b}_l$ and $\mathbf{b}_{nl}$ are the linear and nonlinear differential operators. The complete expression of $\mathbf{b}_l$ and $\mathbf{b}_{nl}$ are different for 1D and 2D models. In the case of 1D model, they read:

$$\mathbf{b}_l = \begin{bmatrix} \partial_x & 0 & 0 \\ 0 & \partial_y & 0 \\ 0 & 0 & \partial_z \\ \partial_z & 0 & \partial_x \\ 0 & \partial_z & \partial_y \\ \partial_y & \partial_x & 0 \end{bmatrix}, \qquad \mathbf{b}_{nl} = \begin{bmatrix} \frac{1}{2}(\partial_x)^2 & \frac{1}{2}(\partial_x)^2 & \frac{1}{2}(\partial_x)^2 \\ \frac{1}{2}(\partial_y)^2 & \frac{1}{2}(\partial_y)^2 & \frac{1}{2}(\partial_y)^2 \\ \frac{1}{2}(\partial_z)^2 & \frac{1}{2}(\partial_z)^2 & \frac{1}{2}(\partial_z)^2 \\ \partial_x\,\partial_z & \partial_x\,\partial_z & \partial_x\,\partial_z \\ \partial_y\,\partial_z & \partial_y\,\partial_z & \partial_y\,\partial_z \\ \partial_x\,\partial_y & \partial_x\,\partial_y & \partial_x\,\partial_y \end{bmatrix} \tag{6}$$

where $\partial_x = \dfrac{\partial(\cdot)}{\partial x}$, $\partial_y = \dfrac{\partial(\cdot)}{\partial y}$, and $\partial_z = \dfrac{\partial(\cdot)}{\partial z}$. For the 2D model, $\mathbf{b}_l$ and $\mathbf{b}_{nl}$ are defined as:

$$\mathbf{b}_l = \begin{bmatrix} \frac{\partial_\alpha}{H_\alpha} & 0 & \frac{1}{H_\alpha R_\alpha} \\ 0 & \frac{\partial_\beta}{H_\beta} & \frac{1}{H_\beta R_\beta} \\ 0 & 0 & \partial_z \\ \partial_z - \frac{1}{H_\alpha R_\alpha} & 0 & \frac{\partial_\alpha}{H_\alpha} \\ 0 & \partial_z - \frac{1}{H_\beta R_\beta} & \frac{\partial_\beta}{H_\beta} \\ \frac{\partial_\beta}{H_\beta} & \frac{\partial_\alpha}{H_\alpha} & 0 \end{bmatrix}, \tag{7}$$

and

$$\mathbf{b}_{nl} = \begin{bmatrix} \frac{1}{2H_\alpha^2}\left[(\partial_\alpha)^2 + \frac{2u_z\partial_\alpha}{R_\alpha} + \frac{u_\alpha}{R_\alpha^2}\right] & \frac{(\partial_\alpha)^2}{2H_\alpha^2} & \frac{1}{2H_\alpha^2}\left[(\partial_\alpha)^2 - \frac{2u_\alpha\partial_\alpha}{R_\alpha} + \frac{u_z}{R_\alpha^2}\right] \\ \frac{(\partial_\beta)^2}{2H_\beta^2} & \frac{1}{2H_\beta^2}\left[(\partial_\beta)^2 + \frac{2u_z\partial_\beta}{R_\beta} + \frac{u_\beta}{R_\beta^2}\right] & \frac{1}{2H_\beta^2}\left[(\partial_\beta)^2 - \frac{2u_\beta\partial_\beta}{R_\beta} + \frac{u_z}{R_\beta^2}\right] \\ \frac{1}{2}(\partial_z)^2 & \frac{1}{2}(\partial_z)^2 & \frac{1}{2}(\partial_z)^2 \\ \frac{1}{H_\alpha}\left(\partial_\alpha\partial_z + \frac{u_z\partial_z}{R_\alpha}\right) & \frac{\partial_\alpha\partial_z}{H_\alpha} & \frac{1}{H_\alpha}\left(\partial_\alpha\partial_z - \frac{u_\alpha\partial_z}{R_\alpha}\right) \\ \frac{\partial_\beta\partial_z}{H_\beta} & \frac{1}{H_\beta}\left(\partial_\beta\partial_z + \frac{u_z\partial_z}{R_\beta}\right) & \frac{1}{H_\beta}\left(\partial_\beta\partial_z - \frac{u_\beta\partial_z}{R_\beta}\right) \\ \frac{1}{H_\alpha H_\beta}\left(\partial_\alpha\partial_\beta + \frac{u_z\partial_\beta}{R_\alpha} + \frac{u_\beta}{R_\alpha R_\beta}\right) & \frac{1}{H_\alpha H_\beta}\left(\partial_\alpha\partial_\beta + \frac{u_z\partial_\alpha}{R_\beta}\right) & \frac{1}{H_\alpha H_\beta}\left(\partial_\alpha\partial_\beta - \frac{u_\alpha\partial_\beta}{R_\alpha} - \frac{u_\beta\partial_\alpha}{R_\beta}\right) \end{bmatrix}, \tag{8}$$

in which $\partial_\alpha = \frac{\partial(\cdot)}{\partial\alpha}$, $\partial_\beta = \frac{\partial(\cdot)}{\partial\beta}$, $H_\alpha = (1 + \frac{z}{R_\alpha})$, and $H_\beta = (1 + \frac{z}{R_\beta})$. Note that Eqs. 7 and 8 are valid for a doubly curved shell, although single curvature structures are considered in this paper. More detail about nonlinear CUF-based shell models can be found in [42].
As far as the constitutive relation is concerned, linear elastic metallic shell structures are considered in this work. Consequently, the constitutive relation reads as:

$$\boldsymbol{\sigma} = \mathbf{C}\boldsymbol{\epsilon}, \tag{9}$$

where and $\mathbf{C}$ is the material elastic matrix, which explicit form can be found in many books, see [43, 44].

2.2 Finite element approximation

The 3D displacement field $\mathbf{u}(x, y, z)$ of the 1D models, within the framework of the Carrera Unified Formulation (CUF), can be expressed as a general expansion of the primary unknowns, as follows:

$$\mathbf{u}(x, y, z) = F_s(x, z)\mathbf{u}_s(y), \qquad s = 1, 2, ..., M \tag{10}$$

where F_s are the functions of the coordinates x and z on the cross-section, $\mathbf{u}_s$ is the vector of the *generalized* displacements which lay along the beam axis, M denotes the order of expansion in the thickness direction, and the summing convention with the repeated index s is assumed. The choice of F_s determines the class of the 1D CUF model that is required and subsequently to be adopted. The research work proposed in this paper makes use of nine-point Lagrange polynomials to approximate the cross-sectional displacement field. As widely shown and demonstrated in [45], this approximated but refined kinematics can describe accurately a wide range of classes of structures. The Finite Element Method (FEM) is adopted to discretize the structure along the y axis. Thus, the generalized displacement vector $\mathbf{u}_s(y)$ is approximated as follows:

$$\mathbf{u}_s(y) = N_j(y)\mathbf{q}_{sj} \qquad j = 1, 2, \ldots, p + 1 \tag{11}$$

where $N_j(y)$ stands for the j-th 1D shape function, p is the order of the shape functions and j indicates summation. $\mathbf{q}_{sj}$ is the following vector of the FE nodal parameters:

$$\mathbf{q}_{sj} = \left\{ \begin{array}{ccc} q_{x_{sj}} & q_{y_{sj}} & q_{z_{sj}} \end{array} \right\}^T \tag{12}$$

For the sake of brevity, the shape functions N_j are not reported here. They can be found in many reference texts, for instance in Bathe [43]. However, it should be underlined that the choice of the cross-section polynomials sets for the LE kinematics is completely independent of the choice of the beam Finite Element (FE) to be used along the beam axis. In this work, classical one-dimensional FEs with four nodes (B4) are adopted, i.e. a cubic approximation along the y axis is assumed.
As far as the 2D models are concerned, through CUF, the 3D displacement field $\mathbf{u}(\alpha, \beta, z)$ can be expanded as a set of thickness functions depending only on the thickness coordinate z and the corresponding variables depending on the in-plane coordinates α and β. Specifically, we have

$$\mathbf{u}(\alpha, \beta, z) = F_s(z)\mathbf{u}_s(\alpha, \beta), \qquad s = 0, 1, \cdots, N, \tag{13}$$

where N is the the order of expansion in the thickness direction. In this work, three-node quadratic (LD2) Lagrange expansion function is adopted. For the sake of generality, FEM is used to discretize the shell structure in the α-β plane. Thus, the generalized displacement vector $\mathbf{u}_s(\alpha, \beta)$ is approximated as follows:

$$\mathbf{u}_s(\alpha, \beta) = N_j(\alpha, \beta)\mathbf{q}_{sj}, \qquad j = 1, 2, \ldots, p+1, \tag{14}$$

where N_j is the j-th shape function, p denotes the order of the shape functions and the repeated index j indicates summation. The vector of the FE nodal parameters $\mathbf{q}_{sj}$ is defined as

$$\mathbf{q}_{sj} = \left\{ \begin{array}{ccc} q_{\alpha_{sj}} & q_{\beta_{sj}} & q_{z_{sj}} \end{array} \right\}^{\mathrm{T}} \tag{15}$$

In this work, the classical 2D nine-node quadratic FEs (Q9) will be adopted for the shape function in the α-β plane. For a better understanding of the proposed models, Fig. 2 reports the approximations previously explained for a generic shell structure adopting 1D beam (Fig. 2(a)) and 2D shell(Fig. 2(b)) models. In particular, the expansion functions F_s, used to approximate the cross-section of the 1D model and the thickness of the 2D shell model, are highlighted in red, whereas the shape functions N_j for the beam axis and the 2D surface are reported in blue.

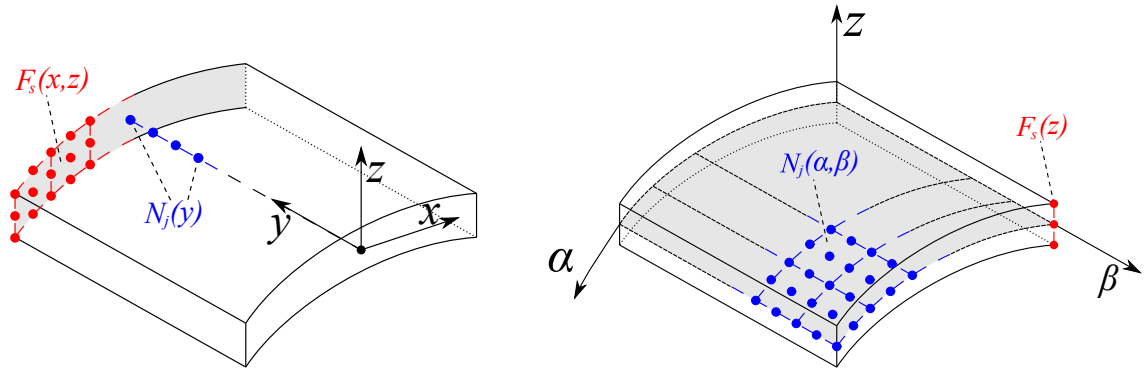

Figure 2: Approximations of the 1D model (a) and 2D model (b) of a generic shell structure.

Finally, introducing the CUF ((Eqs. (10) and (13))) and FEM ((Eqs. (11) and (14))) relations into Eq. (5), the strain vector can be written in algebraic form as follows:

$$\boldsymbol{\epsilon} \;=\; (\mathbf{B}_l^{sj} + \mathbf{B}_{nl}^{sj})\mathbf{q}_{sj} \tag{16}$$

where $\mathbf{B}_l^{sj}$ and $\mathbf{B}_{nl}^{bsj}$ are the linear and nonlinear algebraic matrices with CUF and FEM formulations. The explicit form of these two matrices are not reported here for the sake of brevity, but they are reported in [38] for 1D models, and in [42] for 2D shell models.

3 Nonlinear governing equations

For the evaluation of the nonlinear FE governing equations, consider the principle of virtual work. For a generic body, it reads:

$$\delta L_{\text{int}} = \delta L_{\text{ext}} \tag{17}$$

where δL_{int} is the virtual variation of the strain energy and δL_{ext} is the virtual variation of the work of the external loads. It is important to note that the equations and mathematical steps shown hereafter are suitable for both 1D and 2D models.
The virtual variation of the internal work can be expressed as:

$$\delta L_{\text{int}} = \int_V \delta \boldsymbol{\epsilon}^T \boldsymbol{\sigma} \, \mathrm{d}V \tag{18}$$

where V is the volume of the body. Introducing the geometrical (Eq. (10)) and contitutive relations (Eq. (17)) into Eq. (18), it takes the following form:

$$\delta L_{\text{int}} = \delta \mathbf{q}_{sj}^T \left(\int_V \left(\mathbf{B}_l^{sj} + 2\,\mathbf{B}_{nl}^{sj} \right)^T \mathbf{C} \left(\mathbf{B}_l^{\tau i} + \mathbf{B}_{nl}^{\tau i} \right) \, \mathrm{d}V \right) \mathbf{q}_{\tau i} \tag{19}$$

The argument of the integral of the Eq. (19) represents the so called secant stiffness matrix $\mathbf{K}_S^{ij\tau s}$, so that the equation can be written as:

$$\delta L_{\text{int}} = \delta \mathbf{q}_{sj}^T \mathbf{K}_S^{ij\tau s} \mathbf{q}_{\tau i} \tag{20}$$

The complete form of the secant stiffness matrix $\mathbf{K}_S^{ij\tau s}$ is omitted here for the sake of brevity, but can be found in [38, 46].
The right term of Eq. (17), omitting some mathematical steps, that can be found in Carrera *et al.* [47], can be written as:

$$\delta L_{\text{ext}} = \delta \mathbf{q}_{sj}^T \, \mathbf{p}_{sj} \tag{21}$$

so that Eq. (17) becomes:

$$\mathbf{K}_S^{ij\tau s} \mathbf{q}_{\tau i} - \mathbf{p}_{sj} = 0 \tag{22}$$

Equation (22) can be arbitrarily expanded to reach any desired theory, from low- to higher-order ones, by choosing the values for $\tau, s = 1, 2, \ldots, M$ and $i, j = 1, 2, \ldots, p+1$, to give:

$$\mathbf{K}_S \, \mathbf{q} - \mathbf{p} = 0 \tag{23}$$

where $\mathbf{K}_S$, $\mathbf{q}$, and $\mathbf{p}$ are the global, assembled finite element arrays of the final structure.
Equation (23) represents a nonlinear algebraic system of equation for which an iterative method is needed. We employ here the same procedure detailed in the work by Pagani and Carrera [39], where a Newton-Raphson scheme is derived by making use of a path following constraint. The main steps of the procedure is explained in this work. This procedures demands for the linearization of the nonlinear governing equations. As a result, we need to

introduce the so-called tangent stiffness matrix $\mathbf{K}_T = \dfrac{\mathrm{d}(\mathbf{K}_S\mathbf{q} - \mathbf{p})}{\mathrm{d}\mathbf{q}}$. The explicit form of $\mathbf{K}_T$ is not given here, but it is derived in a unified form in [42]. The resultant system of equations needs to be constrained. In this work, an opportune arc-length path-following constraint is adopted. More detail about the arc-length method adopted can be found in the works by Carrera [48] and Crisfield [49, 50].

4 Numerical results

Various benchmark problems are herein addressed for demonstrating: 1) convergence analyses and comparison between 1D and 2D models; 2) the enhanced capabilities of the proposed 1D and 2D nonlinear refined formulation. Large deflection and quasi-static analyses of cylindrical shell structures are taken into account. The considered cases are inspired from the well-known work by Sze *et al.* [51]. In addition, 3D NASTRAN analyses are conducted for the convergence of the proposed 1D and 2D models.

4.1 Pinched thin-walled cylinder

The capability of the proposed geometrically nonlinear 1D and 2D models is demonstrated by the comparison with the results proposed by Pagani *et al.* [46], where a pinched thin-walled cylinder was analyzed. The material and geometrical properties come from the well-known problem analyzed by Flügge [52]. The material is isotropic with Young modulus $E = 3 \times 10^6$ psi and Poisson ratio $\nu = 0.3$. The geometry is shown in Fig. 3, with length $L = 600$ in, radius $r = 300$ in and thickness $t = 3$ in. The displacement field was evaluated adopting both 1D and

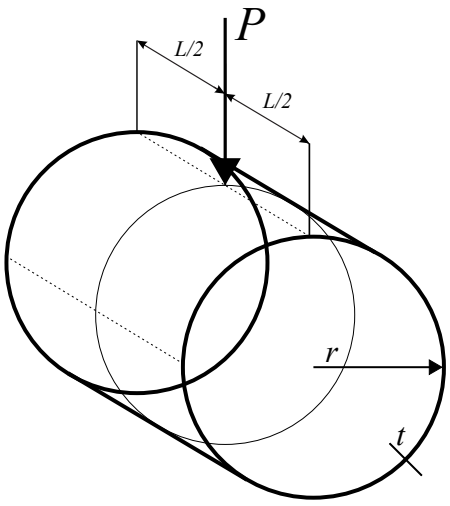

Figure 3: Geometry and loading condition for the pinched thin-walled cylinder.

2D theories in the framework of CUF. As far as the 1D model is concerned, the discretization of the cross-section is reported in Fig. 4(a). 10L9, 20L9, and 30L9 Lagrange polynomials were employed for the evaluation of the 3D displacement field over the cross-section, whereas a cubic interpolation along the y-axis is assumed by introducing 1, 2 and 3 classical 1D FEs with four nodes (B4). Fig. 4(b) shows the 2D shell model, and from 12Q9 up to 600Q9 polynomials were employed for the surface discretization, whereas 1LD2 is employed in the thickness direction.
Figure 5 shows the quasi-static equilibrium curve of the transverse displacement of the point

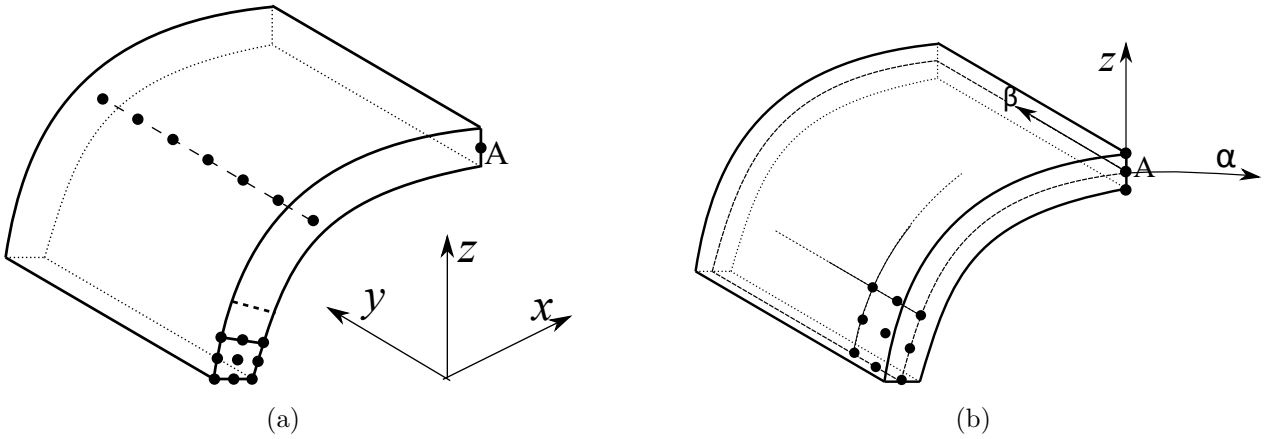

Figure 4: Cross-section approximations of the 1D model (a) and 2D model (b) for the pinched thin-walled cylinder.

A (see Fig. 4). Fig. 5(a) reports the results for the 1D model. Regarding the cross-section, it results clear that the 30L9 discretization represents a reliable approximations, whereas for the beam axis, increasing the number of the elements leads to more accurate results. 30L9/20B4 represents a good discretization for the evaluation of the 3D displacement field. Fig. 5(b) reports the solution for the 2D shell model, and the solution is achieved with a great accuracy starting from 600Q9 elements to describe the kinematic of the surface of the cylinder. Correspondent values are reported in Table 1 and compared with those from the 2D and 3D analysis of NASTRAN. The NASTRAN mesh for both models is depicted in 6. For the 2D model, 5400 shell elements were used, 90 along the circumferential direction and 60 along the length. Each element has thickness t. For the 3D model, 126000 solid elements were used, 315 along the circumferential direction, 200 along the length and 2 for the thickness.

Model	Approximation	DoFs	P = 500.0	P = 1000	P = 1500	P = 2000
			u_{zA}	u_{zA}	u_{zA}	u_{zA}
1D Beam	10L9 + 3B4	1890	30.64	42.35	49.63	55.15
	30L9 + 1B4	2196	28.38	39.00	45.91	51.23
	20L9 + 3B4	3690	32.97	44.30	51.38	57.02
	30L9 + 3B4	5490	33.35	44.72	51.86	57.57
	30L9 + 10B4	17019	34.13	45.86	53.58	59.50
	30L9 + 15B4	25254	34.26	46.14	53.73	59.82
	30L9 + 20B4	33489	**34.49**	**46.89**	**54.21**	**59.92**
2D Shell	12Q9 + 1LD2	567	8.865	26.70	35.71	41.74
	40Q9 + 1LD2	1683	28.08	39.61	47.08	52.70
	70Q9 + 1LD2	2835	30.48	41.85	49.18	54.79
	200Q9 + 1LD2	7749	33.16	44.61	51.99	57.62
	600Q9 + 1LD2	22509	**34.35**	**46.11**	**53.68**	**59.15**
3D NASTRAN	200 × 315	571644	**34.36**	**46.23**	**54.76**	**59.58**

Table 1: Transverse displacement for the 1D and 2D models of the pinched thin-walled cylinder evaluated at the middle of the thickness of the structure (see point A in Fig. 4). P is expressed in klb, u_{zA} in inches.

Subsequently, a comparison between the converged 1D and 2D models and the 3D solution

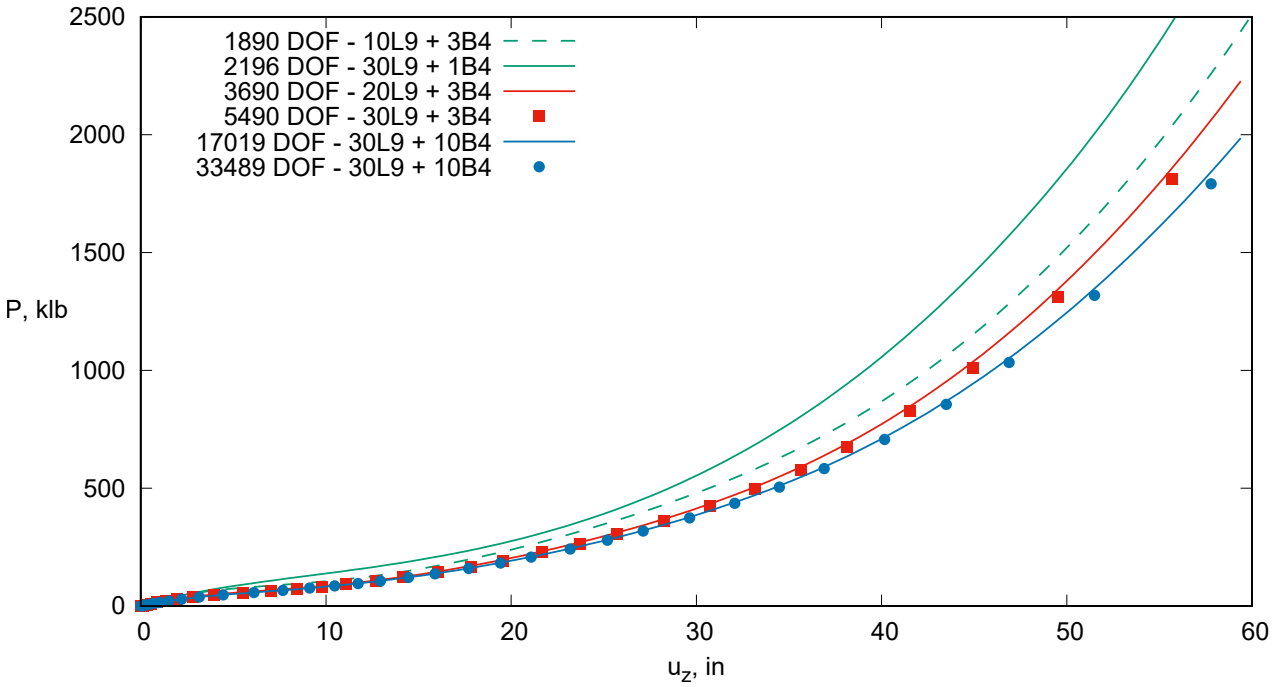

(a) 1D Beam CUF model

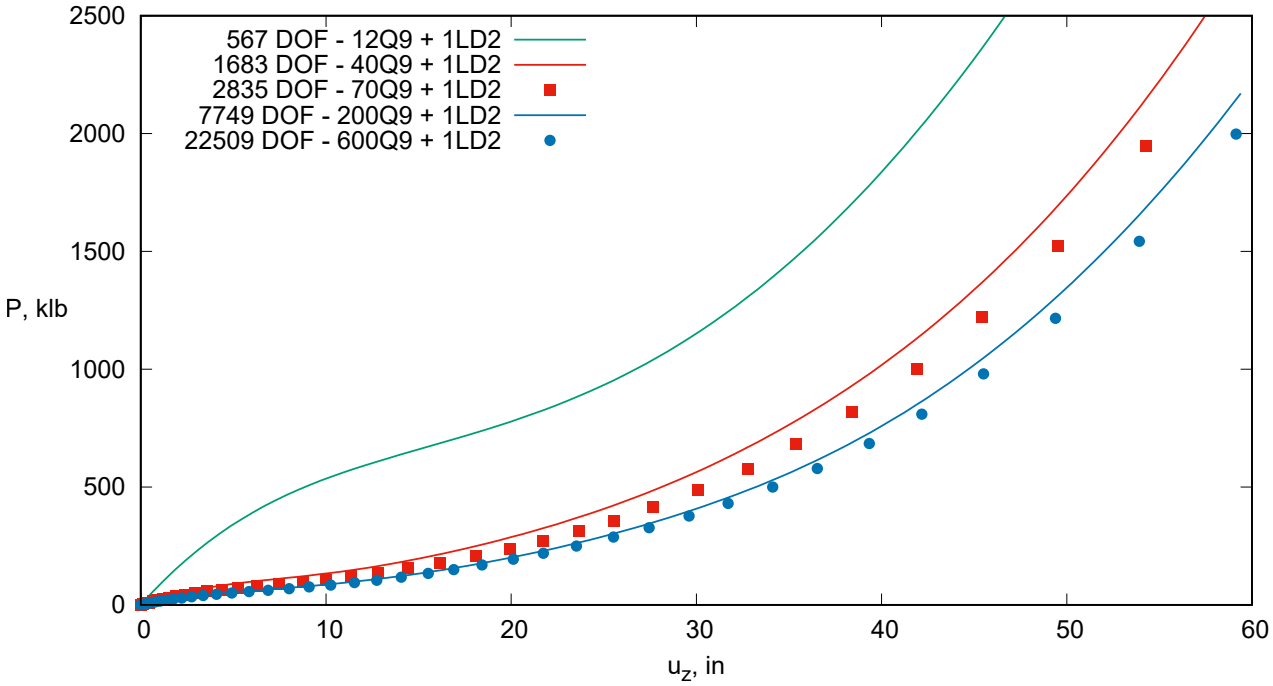

(b) 2D Shell CUF model

Figure 5: Nonlinear equilibrium curves of the pinched thin-walled cylinder using 1D (a) and 2D (b) models. Displacement evaluated at the middle of the thickness of the structure (see point A in Fig. 4). P is expressed in klb, u_z in inches.

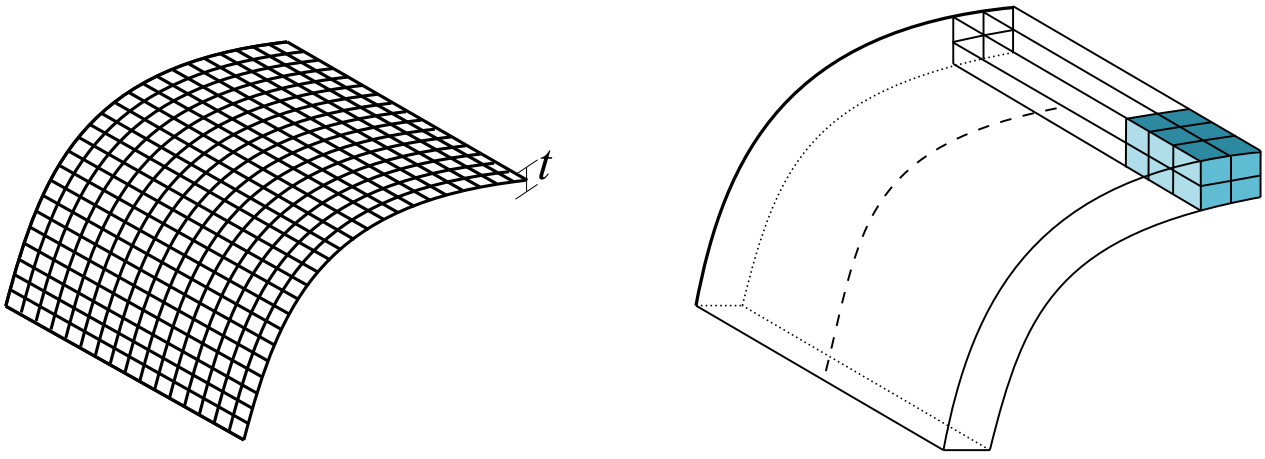

(a) (b)

Figure 6: Mesh of the 2D model (a) and 3D model (b) of NASTRAN for the pinched thin-walled cylinder.

from NASTRAN was made. The results are shown in Fig. 7, and the solution from both models perfectly match the reference one, with 33489 Degrees of Freedom (DoFs) for the 1D model and 22509 DoFs for the 2D model. The convergence analysis between the two models compared to the 3D solution of NASTRAN is shown in Fig. 14. It can be pointed out that the 1D model presents a faster convergence than the shell model. The shown convergence analysis was conducted for $P = 1000$ klb.
As a final analysis, a 1D model with different sizes of the FEs is proposed. In fact, for the results previously shown, a homogeneous discretization for the beam axis is adopted, so that every B4 element has the same size. This choice was made to make the proposed model as more generic as possible and suitable for every loading and boundary condition. However, one of the main features of proposed the unified 1D model is the possibility to refine the mesh in certain zones of interest within the structure without any issues. As depicted in Fig. 10, one can add more FEs in the proximity of interested areas (for example, the external force) without any mesh problems. For the 2D models, the refinement is not possible without resorting to external and time-consuming techniques. Fig. 10(b) shows a finer mesh, and some red nodes are not connected. Next, a 15B4 1D model with a different size of the FEs is considered in the next analysis. To distinguish this analysis from the other, an apex is used, so that 15B4* means that the FEs are not equi-sized. The displacement trend is shown in Fig. 9. Clearly, the results are slightly different from the equi-sized FE mesh, and the 15B4* solution is closer to the previously shown with 20B4, with a significant loss of DoFs. Correspondent values are reported in Table 2.

4.2 Cylindrical hinged panel

As a further example, a cylindrical panel with hinged-free-hinged-free boundary condition is addressed. The analyzed structure comes from the work by Sze *et al.* [51]. The material and geometrical properties are report without any unit of measure, so they are reported hereafter in the same way. The structure is made of an isotropic material with Young modulus $E = 3102.75$ and Poisson ratio $\nu = 0.3$. The geometry is shown in Fig. 11, with length $L = 508$ in, radius $R = 2540$, thickness $t = 12.7$, and $\theta = 0.1$ rad. The sides Ω_1 and Ω_2 are hinged, while the other sides are free. As in the previous study case, both 1D and 2D models were

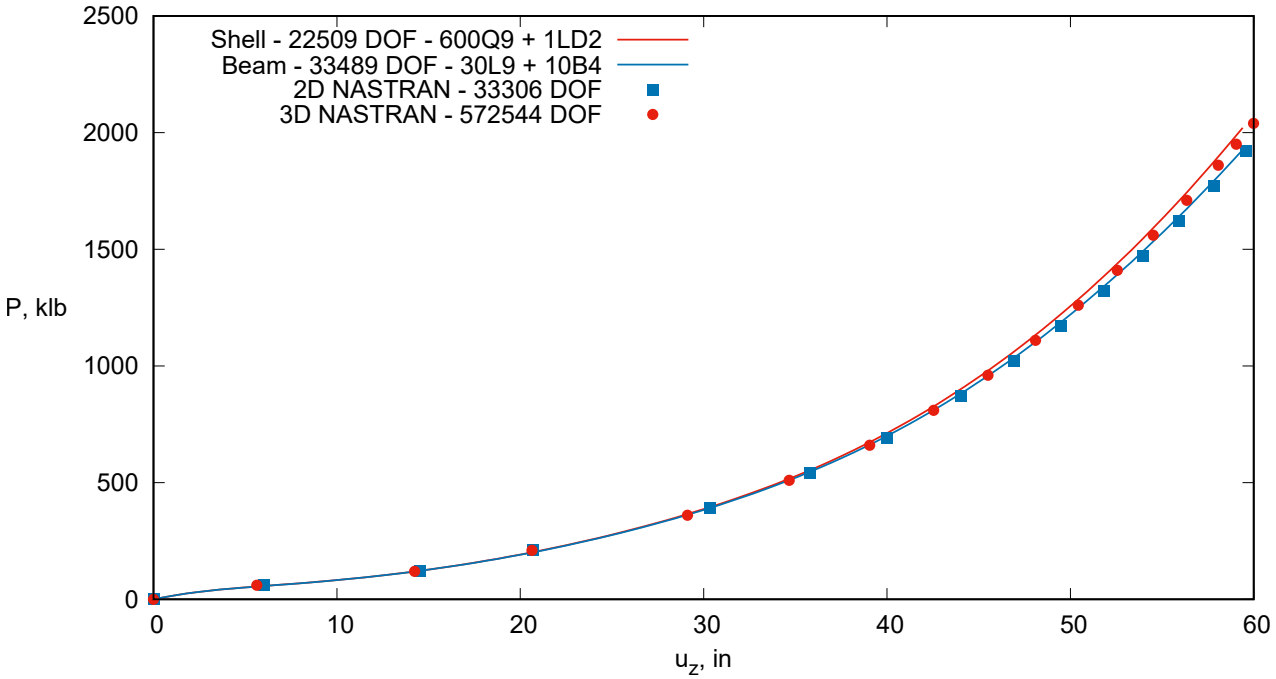

Figure 7: Nonlinear equilibrium curves of the pinched thin-walled cylinder using 1D and 2D converged models compared to 2D and 3D analyses with NASTRAN. Displacement evaluated at the middle of the thickness of the structure (see point A in Fig. 4). P is expressed in klb, u_{zA} in inches.

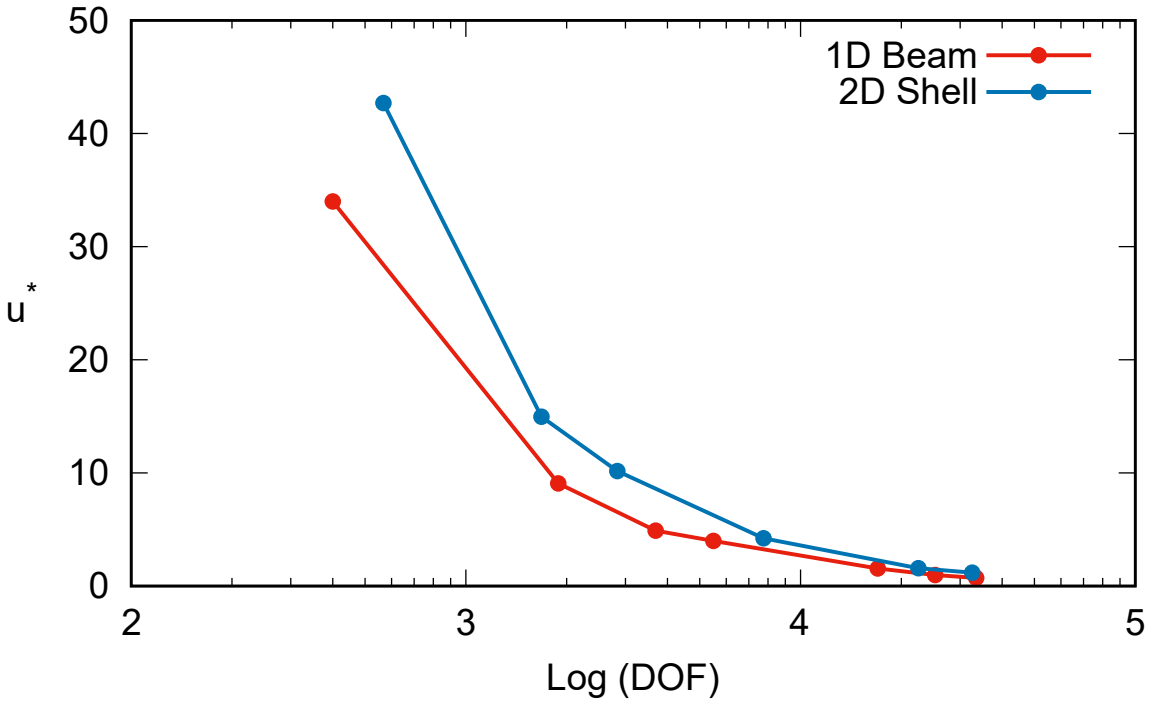

Figure 8: Convergence analysis of 1D beam and 2D shell CUF models of the pinched thin-walled cylinder. Reference solution comes from 3D analysis with NASTRAN. $P = 1000$ klb and $u^* = \dfrac{u_z - u_{z\,Ref.}}{u_{z\,Ref.}}$.

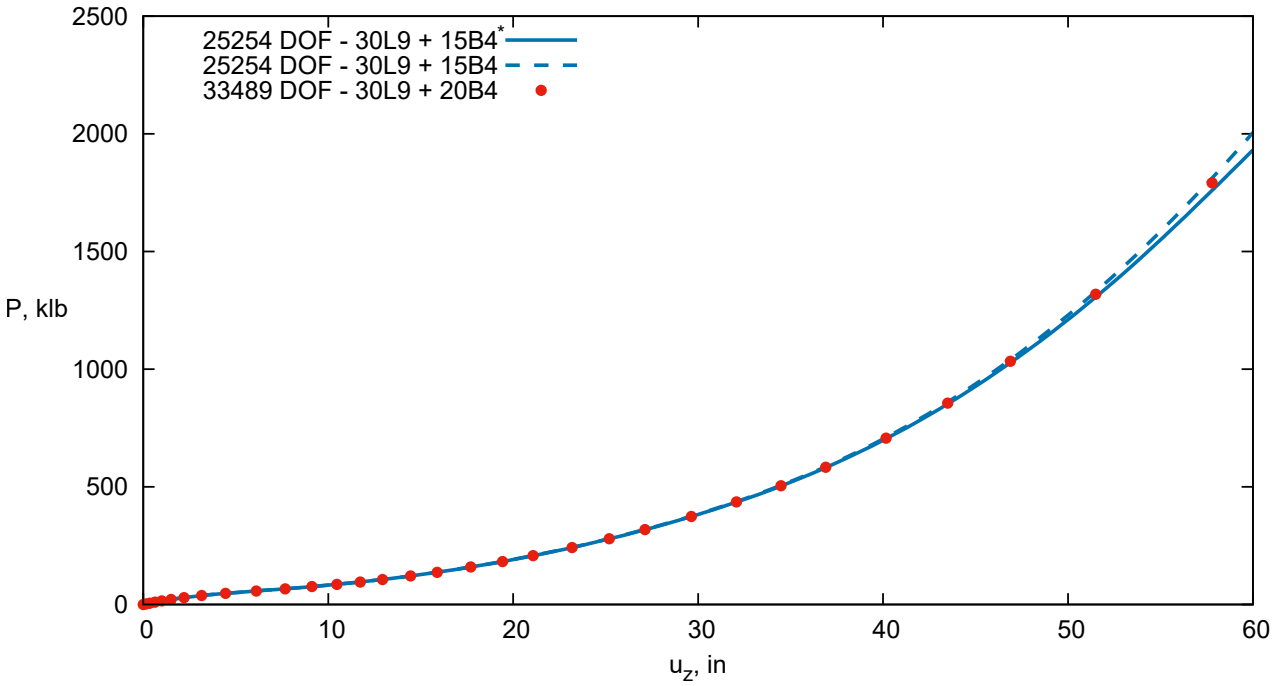

Figure 9: Nonlinear equilibrium curves of the pinched thin-walled cylinder using 1D models. Transverse displacement valuated at the middle of the thickness of the structure (see point A in Fig. 4). 15B4* means that elements along the beam axis do not have the same size, but they are finer near the external force.

Model	Approximation	DoFs	P = 500.0	P = 1000	P = 1500	P = 2000
			u_{zA}	u_{zA}	u_{zA}	u_{zA}
1D Beam	30L9 + 10B4	17019	34.13	45.86	53.58	59.50
	30L9 + 15B4	25254	34.26	46.14	53.73	59.82
	30L9 + 15B4*	25254	34.32	46.32	54.26	60.43
	30L9 + 20B4	33489	34.49	46.89	54.21	59.92
3D NASTRAN	200 × 315	571644	**34.36**	**46.23**	**54.76**	**59.58**

Table 2: Transverse displacement for the 1D model of the pinched thin-walled cylinder evaluated at the middle of the thickness of the structure (see point A in Fig. 4). P is expressed in klb, u_{zA} in inches. 15B4* means that elements along the beam axis do not have the same size, but they are finer near the external force.

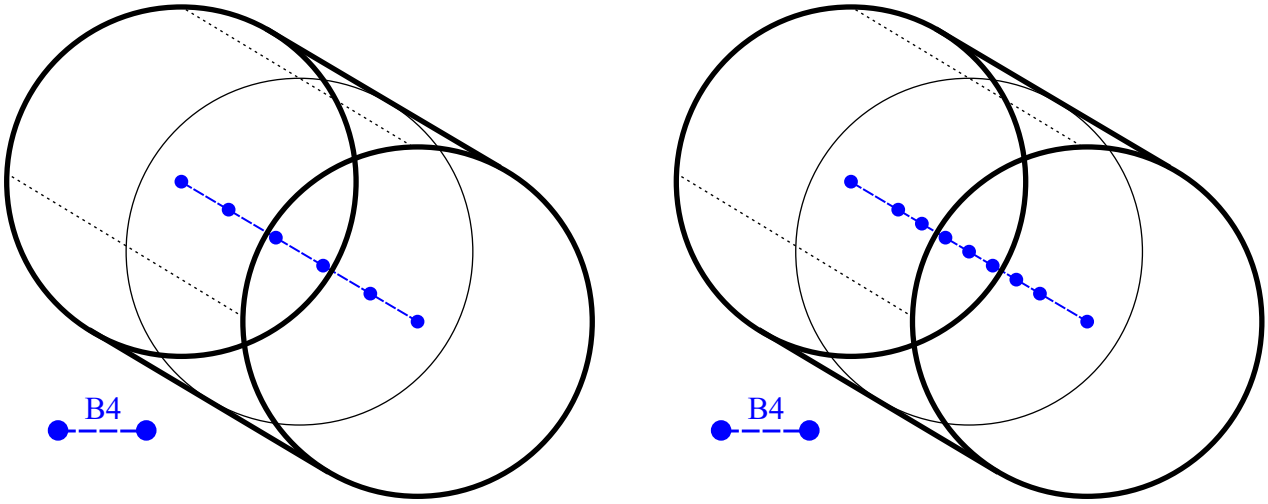

(a)

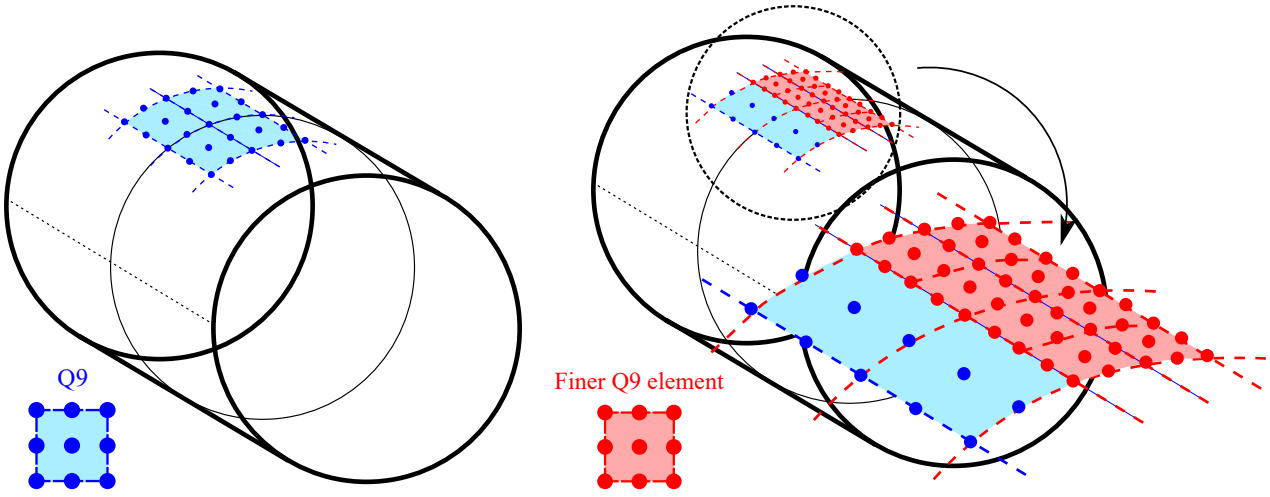

(b)

Figure 10: 1D elements (a) allow for the refinment of the model without any mesh incongruence. 2D elements (b) present lack of nodes connectivity if a finer mesh is employed in portions of the structure.

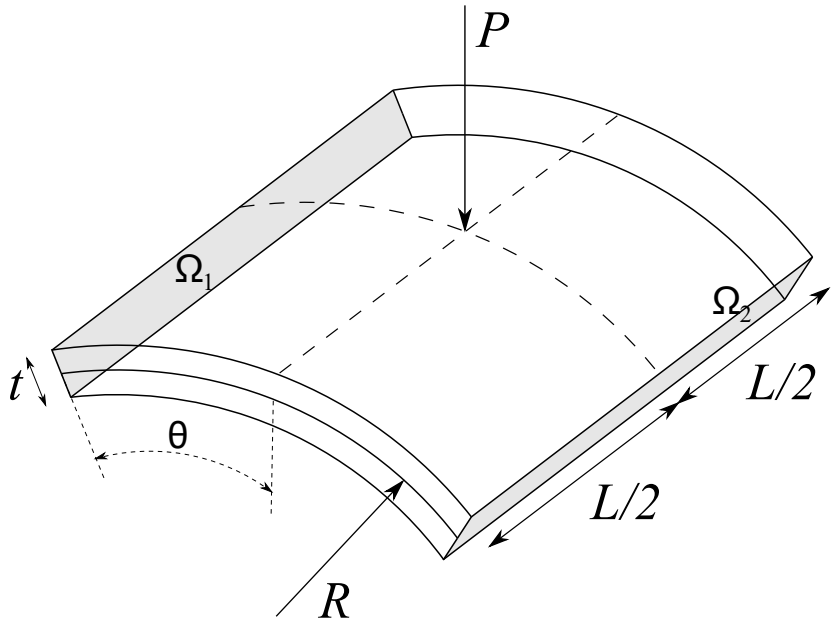

Figure 11: Geometry and loading condition for the cylindrical hinged panel.

used to evaluate the displacement field over the whole panel. From 4 to 10 L9 Lagrange polynomials were employed for the evaluation of the 3D displacement field over the cross-section of the 1D beam model, whereas a cubic interpolation along the y-axis is assumed by introducing 10 B4 FEs. As far as the 2D shell model is concerned, 25, 36 81 and 100 Q9 were employed for the surface approximation, whereas 1LD2 is employed in the thickness direction. Then, the quasi-static nonlinear equilibrium curve was evaluated, and the results are shown in Fig. 12 in terms of the transverse displacement of the middle point of the panel. Figure 5(a) shows the results for the 1D model. Clearly, 8L9 and 10L9 lead to the same results, so 8L9/10B4 is assumed as an enough refined model, whereas the solution from 4L9 and 6L9 slighltly deviate from the converged solution. Figure 5(b) reports the solution for the 2D model, and the solution is achieved with a great accuracy starting from 81Q9 elements to describe the kinematic of the surface of the panel. Correspondent values are reported in Table 3, comparing them to the Reference solution coming from Sze *et al.* [51]. Subsequently, a comparison between the converged 1D and 2D models and the reference solution was made. The results are shown in Fig. 13, and the solution from both models perfectly match the reference one, with 4743 DoFs for the 1D model and 3969 DoFs for the 2D model.

Finally, convergence analysis is shown in Fig. 14. As in the previous analysis case, it can be pointed out that the beam model presents a faster convergence than the shell model, although the two curves overlap near the 3300 DoFs. The shown convergence analysis was conducted for $P = 2000$.

5 Conclusions

The present paper has demonstrated the capability of one-dimensional (1D) and two-dimensional (2D) models comparing results with those from literature or 2D and three-dimensional (3D) models from NASTRAN. The large deflection regime of shell structures has been analyzed. For this purpose, Finite Element (FE) 1D and 2D models have been built within the Carrera Unified Formulation (CUF), which allows the implementation of low- to higher-order theories, including geometrical nonlinear effects. Convergence analyses have been carried out by com-

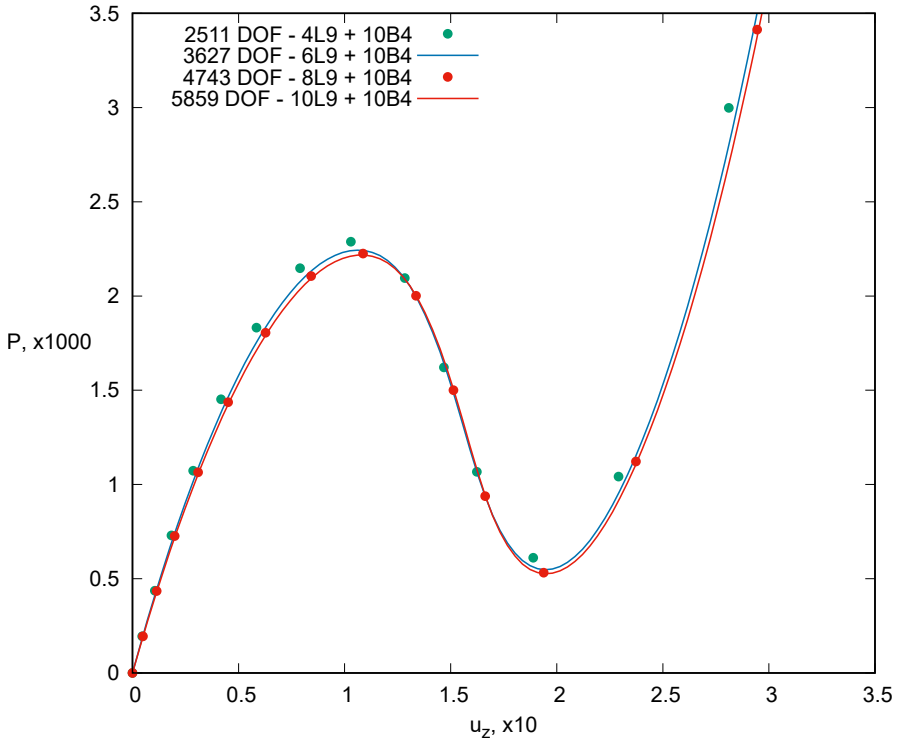

(a) 1D Beam CUF model

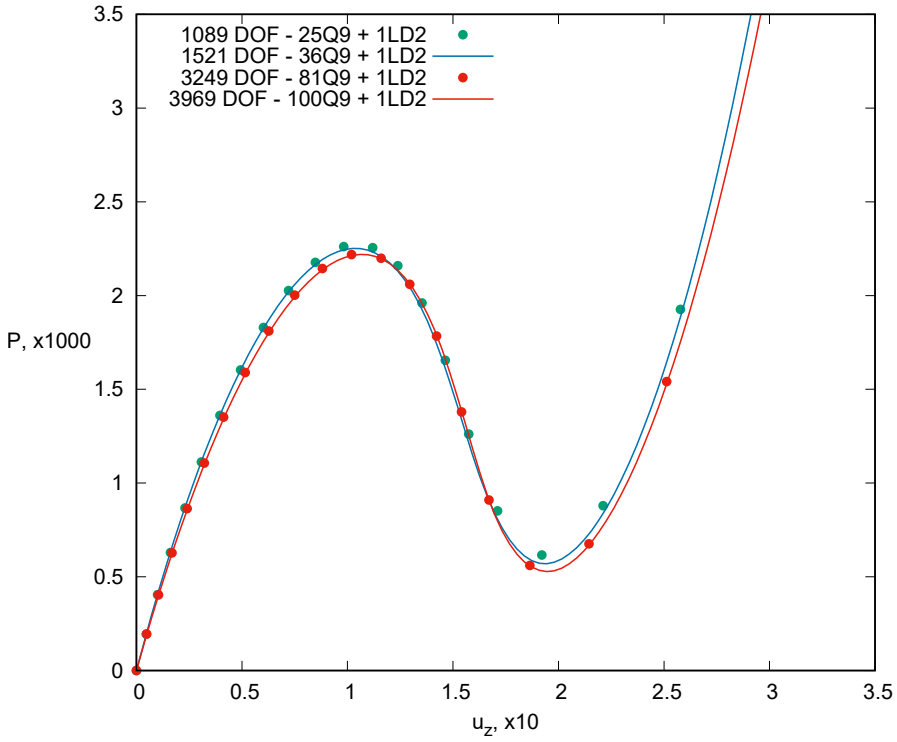

(b) 2D Shell CUF model

Figure 12: Nonlinear equilibrium curves of the pinched thin-walled cylinder using 1D (a) and 2D (b) models. Displacement evaluated at the middle of the thickness of the structure (see point A in Fig. 4). P is expressed in klb, u_{zA} in inches.

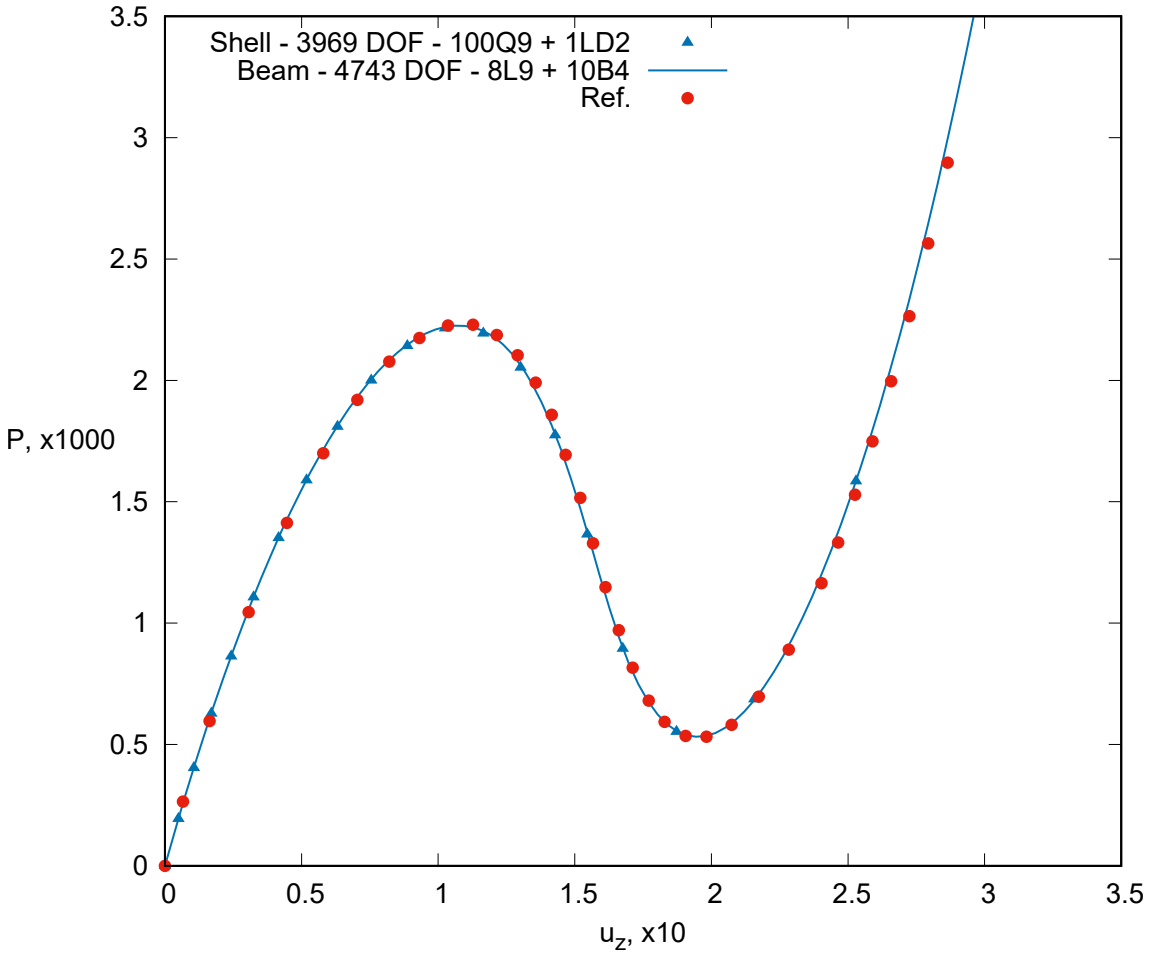

Figure 13: Nonlinear equilibrium curves of the pinched thin-walled cylinder using 1D and 2D converged models compared to the reference solution. P is expressed in N, u_{zA} in mm. Reference solution comes from Sze *et al.* [51].

Model	Approximation	DoFs	P = 1.0	P = 2.0	P = 2.5
			u_{zA}	u_{zA}	u_{zA}
1D Beam	8L9 + 4B4	1989	2.859	7.611	27.29
	4L9 + 10B4	2511	2.642	6.940	26.79
	8L9 + 6B4	2907	2.877	7.649	27.48
	6L9 + 10B4	3627	2.815	7.459	27.06
	8L9 + 8B4	3825	2.883	7.663	27.19
	8L9 + 10B4	4743	2.886	7.671	27.18
	10L9 + 10B4	5859	2.923	7.777	27.23
2D Shell	25Q9 + 1LD2	1089	2.719	7.036	26.85
	36Q9 + 1LD2	1521	2.712	7.080	26.87
	50Q9 + 1LD2	2079	2.776	7.186	26.87
	81Q9 + 1LD2	3249	2.857	7.479	27.18
	100Q9 + 1LD2	3969	**2.884**	**7.550**	**27.25**
Ref.			**2.917**	**7.640**	**27.79**

Table 3: Transverse displacement for the 1D and 2D model of the pinched thin-walled cylinder evaluated at the middle of the thickness of the structure (see point A in Fig. 4). P is expressed in klb, u_{zA} in inches.

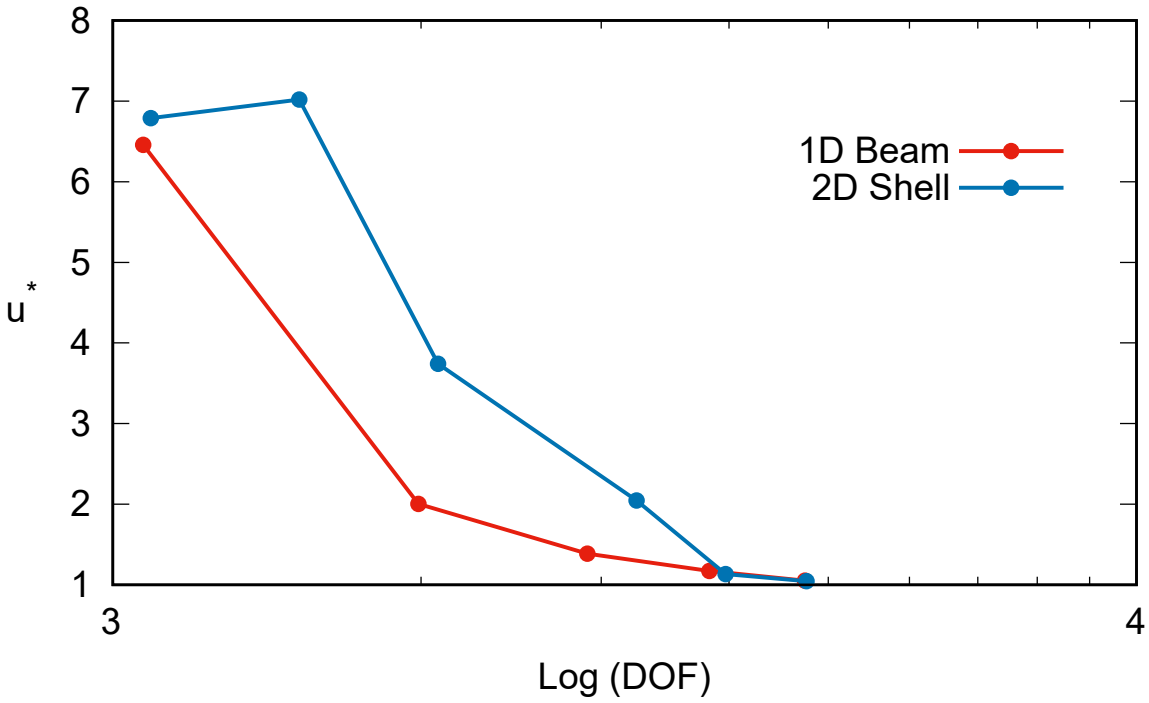

Figure 14: Convergence analysis of 1D beam and 2D shell CUF models of the cylindrical hinged panel. Reference solution comes from Sze *et al.* [51]. $P = 2000$ and $u^* = \frac{u_z - u_{z\,Ref.}}{u_{z\,Ref.}}$.

paring nonlinear quasi-static results with reference ones. Relevant conclusions can be drawn from the obtained results:

- The capability of the unified FE 1D and 2D models to deal with geometrical nonlinear problems is fully demonstrated by comparing obtained results with those from reference and from 3D analysis calculated with NASTRAN;
- Convergence analyses of 1D and 2D models were carried out, and they demonstrate the possibility of 1D models to describe the overall nonlinear behavior of analyzed structure with generally less Degrees of Freedom (DoFs) and, consequently, computational cost than 2D models. Moreover, geometrical relations of 1D models are mathematically way simpler than 2D shell.
- The proposed unified 1D models allows the possibility to refine the discretization in specific parts of the structure, since it is enough to add structural nodes along the beam axis. The same feature is not possible for the 2D models, without resorting to external and time-consuming techniques. This aspect will be further analyzed in future works, including node-dependent kinematics [53] approach, which allows to change the kinematic assumptions node-by-node.

References

[1] L. Euler. *De curvis elasticis*. Lausanne and Geneva: Bousquet, 1744.

[2] S. P. Timoshenko. On the correction for shear of the differential equation for transverse vibrations of prismatic bars. *Philos Mag*, 41(245):744–746, 1921.

[3] S. P. Timoshenko. On the transverse vibrations of bars of uniform cross-section. *Philos Mag*, 43(253):125–131, 1922.

[4] V. V. Novozhilov. *Theory of elasticity*. Pergamon, Elmsford, 1961.

[5] E. Carrera, A. Pagani, M. Petrolo, and E. Zappino. Recent developments on refined theories for beams with applications. *Mech. Eng. Rev.*, 2(2):14–00298, 2015.

[6] R. K. Kapania and S. Raciti. Recent advances in analysis of laminated beams and plates. part i: Shear effects and buckling. *AIAA J.*, 27(7):923–935, 1989.

[7] R. K. Kapania and S. Raciti. Recent advances in analysis of laminated beams and plates. part ii: Vibrations and wave propagation. *AIAA J.*, 27(7):935–946, 1989.

[8] J. N. Reddy. On locking-free shear deformable beam finite elements. *Comput. Methods Appl. Mech. Eng.*, 149(1-4):113–132, 1997.

[9] J. Petrolito. Stiffness analysis of beams using a higher-order theory. *Comput. & Struct.*, 55(1):33–39, 1995.

[10] M. Eisenberger. An exact high order beam element. *Comput. & Struct.*, 81(3):147–152, 2003.

[11] S. Rendek and I. Baláž. Distortion of thin-walled beams. *Thin-walled structures*, 42(2):255–277, 2004.

[12] J. Frischkorn and S. Reese. A solid-beam finite element and non-linear constitutive modelling. *Computer Methods in Applied Mechanics and Engineering*, 265:195–212, 2013.

[13] R. F Vieira, F. B. E. Virtuoso, and E. B. R. Pereira. A higher order beam model for thin-walled structures with in-plane rigid cross-sections. *Eng. Struct.*, 84:1–18, 2015.

[14] A. L. Cauchy. Sur l'equilibre et le mouvement d'une plaque solide. *Exercises Math.*, 3:328–355, 1828.

[15] S. D. Poisson. Mémoire sur l'équilibre et le mouvement des corps élastiques. *Mém. Acad. Sci. Inst. Fr.*, 8:357–570, 1829.

[16] G. Kirchoff. Uber das gleichgewicht und die bewegung einer elastischen scheibe. *J. Reine Angew. Math.)*, 40:51–88, 1850.

[17] A. E. H. Love. *The Mathematical Theory of Elasticity*. Cambridge University Press, Cambridge, 2013.

[18] E. Reissner. The effect of transverse shear deformation on the bending of elastic plates. *J. appl. Mech.*, 12:69–76, 1945.

[19] Raymond D Mindlin. Influence of rotatory inertia and shear on flexural motions of isotropic, elastic plates. *J. appl. Mech.*, 18:1031–1036, 1951.

[20] J. N. Reddy. A simple higher-order theory for laminated composite plates. *Journal of aApplied Mechanics*, 51(4):745–752, 1984.

[21] J. N. Reddy and C. F. Liu. A higher-order shear deformation theory of laminated elastic shells. *International Journal of Engineering Science*, 23(3):319–330, 1985.

[22] S. A. Kulkarni and K. M. Bajoria. Finite element modeling of smart plates/shells using higher order shear deformation theory. *Composite Structures*, 62(1):41–50, 2003.

[23] KM Liew, CW Lim, and S Kitipornchai. Vibration of shallow shells: a review with bibliography. 1997.

[24] T. J. R. Hughes and W. K. Liu. Nonlinear finite element analysis of shells: Part i. three-dimensional shells. *Comput. Methods Appl. Mech. Eng.*, 26(3):331–362, 1981.

[25] K. S. Surana. Geometrically nonlinear formulation for the curved shell elements. *Int. J. Numer. Methods Eng.*, 19(4):581–615, 1983.

[26] Thomas J. R. Hughes and E. Carnoy. Nonlinear finite element shell formulation accounting for large membrane strains. *Computer Methods in Applied Mechanics and Engineering*, 39(1):69–82, 1983.

[27] H. C. Park, C. Cho, and S. W. Lee. An efficient assumed strain element model with six dof per node for geometrically non-linear shells. *Int. J. Numer. Methods Eng.*, 38(24):4101–4122, 1995.

[28] S. J. Lee and W. Kanok-Nukulchai. A nine-node assumed strain finite element for large-deformation analysis of laminated shells. *Int. J. Numer. Methods Eng.*, 42(5):777–798, 1998.

[29] E. Providas and M. A. Kattis. A simple finite element model for the geometrically nonlinear analysis of thin shells. *Comput. Mech.*, 24(2):127–137, 1999.

[30] E. Carrera, G. Giunta, and M. Petrolo. *Beam Structures: Classical and Advanced Theories*. John Wiley & Sons, 2011.

[31] E. Carrera, M. Cinefra, M. Petrolo, and E. Zappino. *Finite Element Analysis of Structures through Unified Formulation*. John Wiley & Sons, Chichester, West Sussex, UK., 2014.

[32] E. Carrera, M. Filippi, P. K. Mahato, and A. Pagani. Accurate static response of single- and multi-cell laminated box beams. *Composite Structures*, 136:372–383, 2016.

[33] M. Filippi and E. Carrera. Capabilities of 1d cuf-based models to analyze metallic/composite rotors. In *8th Australasian Congress on Applied Mechanics: ACAM 8*, page 315. Engineers Australia, 2014.

[34] E. Carrera and A. Pagani. Free vibration analysis of civil engineering structures by component-wise models. *Journal of Sound and Vibration*, 333(19):4597–4620, 2014.

[35] E. Carrera, M. Petrolo, and A. Varello. Advanced beam formulations for free-vibration analysis of conventional and joined wings. *Journal of Aerospace Engineering*, 25(2):282–293, 2011.

[36] A. Pagani, M. Petrolo, G. Colonna, and E. Carrera. Dynamic response of aerospace structures by means of refined beam theories. *Aerospace Science and Technology*, 46:360–373, 2015.

[37] F. Miglioretti and E. Carrera. Application of a refined multi-field beam model for the analysis of complex configurations. *Mechanics of Advanced Materials and Structures*, 22(1-2):52–66, 2015.

[38] A. Pagani and E. Carrera. Unified formulation of geometrically nonlinear refined beam theories. *Mechanics of Advanced Materials and Structures*, 2016. In Press.

[39] A. Pagani and E. Carrera. Large-deflection and post-buckling analyses of laminated composite beams by carrera unified formulation. *Composite Structures*, 170:40–52, 2017.

[40] A. Pagani, R. Augello, and E. Carrera. Frequency and mode change in the large deflection and post-buckling of compact and thin-walled beams. *Journal of Sound and Vibration*, 432:88–104, 2018.

[41] E. Carrera, A. Pagani, and R. Augello. Effect of large displacements on the vibration response of composite beams. *Submitted*.

[42] B. Wu, G. H. Li, A. Pagani, W. Q. Chen, and E. Carrera. Geometrically nonlinear refined shell theories by carrera unified formulation. *Submitted*.

[43] K. J. Bathe. *Finite Element Procedure*. Prentice hall, Upper Saddle River, New Jersey, USA, 1996.

[44] T. J.R. Hughes. *The Finite Element Method: Linear Static and Dynamic Finite Element Analysis*. Courier Corporation, 2012.

[45] E. Carrera and M. Petrolo. Refined beam elements with only displacement variables and plate/shell capabilities. *Meccanica*, 47(3):537–556, 2012.

[46] E. Carrera, A. Pagani, and R. Augello. Evaluation of geometrically nonlinear effects due to large cross-sectional deformations of compact and shell-like structures. *Mechanics of Advanced Materials and Structures*, pages 1–9, 2018.

[47] E. Carrera, G. Giunta, and M. Petrolo. *Beam structures: classical and advanced theories*. John Wiley & Sons, New York, USA, 2011.

[48] E. Carrera. A study on arc-length-type methods and their operation failures illustrated by a simple model. *Computers & structures*, 50(2):217–229, 1994.

[49] M. A. Crisfield. A fast incremental/iterative solution procedure that handles "snap-through". In *Computational Methods in Nonlinear Structural and Solid Mechanics*. Elsevier, Amsterdam, Netherlands, 1981.

[50] M. A. Crisfield. An arc-length method including line searches and accelerations. *International journal for numerical methods in engineering*, 19(9):1269–1289, 1983.

[51] K. Y. Sze, X. H. Liu, and S. H. Lo. Popular benchmark problems for geometric nonlinear analysis of shells. *Finite elements in analysis and design*, 40(11):1551–1569, 2004.

[52] W. Flügge. *Stresses in shells*. Springer, Berlin, 2nd edition, 1960.

[53] E. Carrera and E. Zappino. One-dimensional finite element formulation with node-dependent kinematics. *Computers & Structures*, 192:114–125, 2017.